South China Sea Wave Characteristics during Typhoon Muifa Passage in Winter 2004

Peter C. Chu and Kuo-Feng Cheng

Naval Ocean Analysis and Prediction Laboratory
Department of Oceanography Naval Postgraduate School, Monterey, CA 93943

Report Documentation Page

Form Approved
OMB No. 0704-0188

Public reporting burden for the collection of information is estimated to average 1 hour per response, including the time for reviewing instructions, searching existing data sources, gathering and maintaining the data needed, and completing and reviewing the collection of information. Send comments regarding this burden estimate or any other aspect of this collection of information, including suggestions for reducing this burden, to Washington Headquarters Services, Directorate for Information Operations and Reports, 1215 Jefferson Davis Highway, Suite 1204, Arlington VA 22202-4302. Respondents should be aware that notwithstanding any other provision of law, no person shall be subject to a penalty for failing to comply with a collection of information if it does not display a currently valid OMB control number.

1. REPORT DATE	2. REPORT TYPE	3. DATES COVERED
2008		**00-00-2008 to 00-00-2008**

4. TITLE AND SUBTITLE	5a. CONTRACT NUMBER
South China Sea Wave Characteristics During Typhoon Muifa Passage in Winter 2004	5b. GRANT NUMBER
	5c. PROGRAM ELEMENT NUMBER
6. AUTHOR(S)	5d. PROJECT NUMBER
	5e. TASK NUMBER
	5f. WORK UNIT NUMBER
7. PERFORMING ORGANIZATION NAME(S) AND ADDRESS(ES) **Naval Postgraduate School,Department of Oceanography,Monterey,CA,93943**	8. PERFORMING ORGANIZATION REPORT NUMBER
9. SPONSORING/MONITORING AGENCY NAME(S) AND ADDRESS(ES)	10. SPONSOR/MONITOR'S ACRONYM(S)
	11. SPONSOR/MONITOR'S REPORT NUMBER(S)

12. DISTRIBUTION/AVAILABILITY STATEMENT
Approved for public release; distribution unlimited

13. SUPPLEMENTARY NOTES

14. ABSTRACT

15. SUBJECT TERMS

16. SECURITY CLASSIFICATION OF:			17. LIMITATION OF ABSTRACT	18. NUMBER OF PAGES	19a. NAME OF RESPONSIBLE PERSON
a. REPORT **unclassified**	b. ABSTRACT **unclassified**	c. THIS PAGE **unclassified**	**Same as Report (SAR)**	**48**	

Abstract

Ocean wave characteristics in the western Atlantic Ocean (Hurricane Region) to tropical cyclones have been investigated extensively, but not the regional seas in the western Pacific such as the South China Sea (Typhoon Region). This is due to the lack of observational and modeling studies in western Pacific regional seas. To fill this gap, Wavewatch-III (WW3) is used to study the response of the South China Sea (SCS) to Typhoon Muifa (2004). The WW3 model is integrated from the JONSWAP wave spectra (Hasselmann et al. 1973, 1980) using NASA Quikscatter winds and tropical cyclone wind profile model during Typhoon Muifa passage from 0000UTC 16 on November to 1200UTC on 25 November 2004. This study shows strong similarities in the responses between Hurricane and Typhoon Regions, including strong asymmetry in the significant wave height (H_s) along the typhoon translation track with the maximum H_s in the right-front quadrant of the typhoon center, and asymmetry in the directional wave spectra at different locations (frontward, backward, rightward, leftward) around the typhoon center. The unique features of the SCS wave characteristics to Muifa are also discussed.

1. Introduction

A moving tropical cyclone is an intense source of surface wind stress that causes many significant changes in the ocean wave characteristics such as the significant wave height, directional wave spectra, and wave propagation. These features have been well identified in open oceans in the western Atlantic/eastern Pacific regional seas, that is, the Hurricane Region (hereafter referred to HR). A hurricane with intense and fast-varying winds produces a severe and complex ocean wave field that can propagate for thousands of kilometers away from the storm center, resulting in dramatic variation of the wave field in space and time (Barber and Ursell 1948). To investigate the wave characteristics, the directional spectra of hurricane generated waves were measured using various instruments. For example, the fetch effect was detected in the Celtic Sea using the high-frequency radar. The wave characteristics were obtained for the northeast Pacific during passage of storm using the synthetic aperture radar image from ERS-1 satellite (Holt et al. 1998). The spatial wave variation of hurricane directional wave spectra were identified for both open ocean and landfall cases using the NASA scanning radar altimeter (Wright et al. 2001; Walsh et al. 2002). Hwang and Wang (2001) computed the directional wave spectra from the ocean surface topography.

The ocean wave response identified in HR is a significant right-forward-quadrant bias in the significant wave height. During the passage of Hurricane Bonnie (1998) in the Atlantic Ocean, both observational (Wright et al. 2001) and modeling (Moon et al. 2003) studies show that the significant wave height reaches 14 m in the open ocean. The maximum wave heights appear in the right forward quadrant of the hurricane center and propagate in the same direction as the hurricane. Moon et al. (2003) simulated the wave characteristics successfully using the wave model

WAVEWATCH-III (hereafter referred to WW3) and found that the hurricane-generated wave field is mostly determined by two factors: the distance from the hurricane center or radius of maximum winds (RMW, represented by R_{max}) and hurricane translation speed. For the case of a hurricane with low translation speed, the dominant wave direction is mainly determined by the distance from the hurricane center. However, most of the observational and modeling studies on ocean waves generated by tropical cyclones are focused in HR. Few observational and/or modeling studies have been conducted in the Typhoon Region (hereafter referred to TR), especially in the South China Sea (SCS).

The SCS is one of the largest marginal seas of the Western Pacific Ocean, extending across both tropical and subtropical zones and encompasses a total surface area of 3.5×10^6 km^2 (Figure 1). Also due to its semi-enclosed nature, the SCS is subject to high spatial and temporal variability from external forcing factors. One significant source of the SCS variability is the tropical cyclones that routinely affect the region. The WW3 has been implemented and verified for the SCS using the TOPEX/POSEIDON (T/P) satellite data (Chu et al., 2004). Our goal in this study is to identify if those effects occurring in HR still exist in TR. More specifically, we study the SCS responses to Typhoon Muifa (2004) using WW3.

The outline of the paper is as follows. Section 2 describes movement of typhoon Muifa 2004 over the SCS. Section 3 delineates the establishment of the wind data using the NASA QuikScat (QSCAT) Level 3 data and the tropical cyclone wind profile model (TCWPM). Section 4 depicts the WW3 model. Section 5 describes significant wave height. Section 6 presents the directional wave spectra. Sections 7 and 8 show the effects of typhoon translation speed and intensity on the wave characteristics, and Section 9 gives the conclusions.

2. Typhoon Muifa 2004

Typhoon (TY) Muifa is one of the four tropical cyclones passing by the SCS in 2004. It was formed on 11 November and weakened over land on 26 November. The best track passage of TY Muifa (Figure 2) and best track record (Table 1) were provided by the Joint Typhoon Warning Center (JTWC 2005). The translation speed of TY Muifa is calculated from the distance between typhoon center positions reported by JTWC (Table 2).

2.1. Forming over the Western Pacific

TY Muifa was first generated as a tropical depression on 11 November 2004 in the Western North Pacific Ocean. It moved steadily northwestward passing north of Palau before entering the Philippine Sea. The disturbance was first mentioned by JTWC at 1600UTC 13 November, approximately 400 km north of Palau. The depression was developed into a tropical storm on 14 November. According to its strength, the Japan Meteorological Agency first named it Muifa. However, the Philippine Atmospheric, Geophysical, and Astronomical Services Administration assigned the name Unding at 0000UTC 14 November after the tropical cyclone had invaded their area of responsibility.

Tropical Storm (TS) Muifa was steadily upgraded and moving west-northwestward to the Philippines. It began the clockwise loop at 1200UTC 17 November and continued for several days. On 18 November, the intensity of TY Muifa reached the maximum intensity at 54.0 m/s (115 knots) at 1200UTC and then began a remarkable weakening phase.

2.2. Entering the SCS

TY Muifa was weakened further to 48.9 m/s (95 knots) at 0000UTC 19 November and slowly headed towards southwest. It moved south-southwestward slowly across Luzon and entered

the SCS. Its intensity was weakened to 30.9 m/s (60 knots) and downgraded to a tropical storm at 0600UTC 20 November.

At 0000UTC 21 November, TS Muifa was intensified to 33.4 m/s (65 knots) and upgraded back to typhoon. Further strengthening occurred as TY Muifa went west-southwestwards across the warm waters of the SCS. The intensity of TY Muifa reached the second peak 46.3 m/s (90 knots) at 1800UTC at (11.6^{o}N, 114.4^{o}E), approximately 800 km east of Vietnam. TY Muifa continued its journey to Vietnam from 22 to 23 November and was weakened again. The maximum velocity was further decreased to 23.2 m/s (45 knots) at 1200UTC 24 November.

2.3. Weakening

Muifa was weakened to 15.4 m/s (30 knots) and downgraded to tropical depression status at 1200UTC 25 November. At 0000UTC 26 November Muifa turned northward into an environment of increased wind shear and as the intensity had fallen to 12.9 m/s (25 knots), JTWC issued the final warning on TC Muifa. The final position was 250 km south-southwest of Bangkok, Thailand.

2.4. Typical Locations along the Typhoon Track

Along the track of the TY Muifa passage, the translation velocity, low pressure, intensity, and bathymetry vary (Figure 3). Four locations along the TY passage are selected (Figure 4) to investigate the effect of bottom topography and intensity and translation speed of TY Muifa on the wave characteristics: L-I (arriving the SCS), L-II (strengthening and slowing), L-III (weakening), and L-IV (shelf breaking).

The TY Muifa center was located at L-I (11.9^{o}N, 117.2^{o}E) at 0000UTC on November 21 just after it entered the SCS 24 hr ago. The typhoon translation speed slightly decreased to 5.8 m/s.

The typhoon low pressure was 976 μPa with the maximum wind speed was 33.4 m/s. The estimated RMW is 24.4 km.

The TY Muifa center was located at L-II (11.6°N, 114.4°E) at 1800UTC on 21 November when it reached the strongest intensity (i.e. the lowest center pressure, 954 μPa). The maximum wind speed was 46.3 m/s, and RMW was 14.0 km. The typhoon translation speed slowed down to 4.2 m/s.

The TY Muifa center was located at L-III (10.5°N, 112.1°E) at 0000UTC on 23 November when it had the same intensity as at L-I. The translation speed is notably slower at L-III (3.0 m/s) than at L-I (5.8 m/s). The maximum velocity radius is slightly larger at L-III (RMW = 28.6 km) than at L-I (RMW = 24.4 km). Other conditions are the same at L-III (minimum pressure: 976 μPa, maximum wind speed: 33.4 m/s) as at L-I. L-III is for the typhoon weakening period. Comparison of wave characteristics between L-I and L-III leads to the effect of the translation speed.

The TY Muifa center was located at L-IV (8.8°N, 108.8°E) at 0600UTC on 24 November where TY Muifa (8.8°N, 108.8°E) was close to the Asian landmass. The water depth is about 116 m. The low pressure is 987 μPa, the maximum wind speed was 25.7 m/s with RMW of 40.4 km. The typhoon intensity is much weaker at L-IV than at L-II.

3. Typhoon Winds

During the typhoon seasons, in-situ measurements are difficult to conduct. Remotely sensed data are generally used. The NASA QuikScat (QSCAT) Level 3 data were downloaded during the period of TY Muifa (2004). The evolution of QSCAT wind fields from 17 November to 25 November (Figure 5) clearly show that the typhoon strength agrees properly with the

progressing of TY Muifa into SCS, but the structure of tropical cyclone winds is not presented well due to both the temporal limitation of satellite pass and the inaccurate of scatterometer in high wind speeds.

Due to the spatial coverage, the strong rotational motion from TY Muifa may not be represented in the QSCAT data (Figure 50). To overcome this deficiency, a Tropical Cyclone Wind Profile Model (TCWPM) (Carr and Elsberry 1997) is used to produce the high resolution gridded surface wind field for TY Muifa.

3.1. Tropical Cyclone Wind Profile Model

A tropical cyclone wind profile model (TCWPM) (Carr and Elsberry 1997) is used to establish a high-resolution surface wind field for TY Muifa 2004. Let (R_s, R_0) be the radius of scale, and radius of zero tangential velocity inside a tropical cyclone. Based on the angular momentum balance, Carr and Elsberry (1997) proposed a model to compute the wind vector relative to the center of the tropical cyclone,

$$v_c(r) = \frac{f_0}{2}\left[R_0 \left(\frac{R_0}{r} \right)^X - r \right] \frac{a^4}{1+a^4}, \quad u_c(r) = \tan(\gamma) v_c(r), \tag{1}$$

where r is the horizontal distance to the storm center; (u_c, v_c) are the radial and tangential velocity components; γ is the inflow angle of the wind as it spirals into the center of the cyclone; a is a scaling factor ($a = r/R_s$) that makes $v_c(r)$ continuous at the center of the tropical cyclone; X is a positive constant less than 1. Considering the beta effect propagation, Carr and Elsberry (1997) proposed a value of $X = 0.4$.

To prevent a large discontinuity at the periphery of the storm however, the background wind field ($\mathbf{V}_{bg}$) is blended into the tropical storm wind field. Let $\mathbf{V}_c = (v_c, u_c)$ be the wind vector

relative to the TY center and $\mathbf{V}_t$ be the translation velocity (Table 2). Adjustments were made near the storm's periphery to smooth the transition between the background and storm wind fields. This was done by a weighted average inside and outside of the tropical cyclone,

$$\mathbf{V} = (1-\varepsilon)(\mathbf{V}_c + \mathbf{V}_t) + \varepsilon \mathbf{V}_{bg} \tag{2}$$

where ε is the weight

$$\varepsilon = \frac{c^4}{1+c^4}, \qquad c = \frac{r}{0.9R_0}. \tag{3}$$

The effects of these adjustments are to increase the weighting on the storm wind gradually and decrease the weighting on the background winds as the radial distance to the storm center decreases. Both effects provide for a smoother transition between the storm wind field and the background wind field.

3.2. Determination of Model Parameters

In TCWPM, as described in (1), the tangential wind depends on (r, R_s, R_0). Carr and Elsberry (1997) determine R_0 from the satellite image according to the size of overall convective and outflow cloud pattern of the TC. On the other hand, Chu et al. (2000) fixed the values of radii for the whole typhoon passage. Since there is no satellite image available during TY Muifa passage in the SCS, the values of radii of TY Muifa are determined using the data from Table 1. Near the typhoon center, the winds reported by JTWC can be approximately taken as the tangential winds. Let tangential winds at $(r_1, r_2, ..., r_k)$ be $(v_1, v_2, ..., v_k)$. Eq.(1) gives a set of nonlinear algebraic equations

$$
\begin{aligned}
&v(r_1, R_0, R_s) = v_1, \\
&v(r_2, R_0, R_s) = v_2, \\
&\ldots\ldots, \\
&v(r_k, R_0, R_s) = v_k.
\end{aligned}
\tag{4}
$$

An optimization scheme is used to determine the values of (R_s, R_0), and further to compute $R_{\max}$ from (4). For example, (R_s, R_0) are estimated as (23.7 km, 795 km) at 0600UTC 24 November.

3.3. Background Winds

The background wind vector term (V_{bg}) is obtained by averaging both ascending and descending passes of the QSCAT dataset from November 16 to November 25. The mean wind pattern (Figure 6) shows the dominant winter monsoon with average wind speed of 7.8 m/s.

When the background wind vector term ($\mathbf{V}_{bg}$) in (1) is taken as the temporally averaged QSCAT Level 3 winds from both ascending and descending passes during 16-25 November 2004 (Figure 6). The winds blow from northeast to southwest with the spatial average of about 7.8 m/s. It represents the dominant winter monsoon during the period of TY Muifa passage in the SCS.

3.4. QSCAT-TCWPM Winds

With the mean QSCAT wind data as $\mathbf{V}_{bg}$, the total wind field is computed from 0000UTC on 16 November to 0600UTC on 25 November for (0^o-25^oN, 105^oE-122^oE) using Eq.(1) on a $1/4^\circ \times 1/4^\circ$ grid with the time interval of 6 hr. Such a wind field is referred to the QSCAT-TCWPM (QTCWPM) winds. The daily evolution of the QTCWPM winds (Figure 70) shows that the wind speed increases as TY Muifa enters the SCS, and decreases as Muifa approaches the land. The QTCWPM maximum wind speed is comparable to the maximum wind speed reported in the

best track record (46.3 m/s). Furthermore, the QTCWPM wind field shows asymmetric with the higher wind speed in the right side. The root mean square error is 3.4 m/s between QTCWPM and QSCAT winds. During TY Muifa passage in the SCS, the averaged wind speed is around 35 m/s, the computed QTCWPM wind field is reasonably well.

4. WW3 Model

4.1. Description

The wave spectrum F is generally a function of all phase parameters (i.e., wave number k, direction , intrinsic frequency σ, and absolute frequency ω), space (**x**), and time (t),

$$F = F(k, \ , \sigma, \omega; \mathbf{x}, t). \tag{5}$$

However, the individual spectral components are usually assumed to satisfy the linear wave theory (locally) and to follow the dispersion relation,

$$\sigma^2 = gk \tanh kd \ , \quad \omega = \sigma + \mathbf{k} \bullet \mathbf{U}, \tag{6}$$

where d is the mean water depth and **U** is the (depth- and time- averaged) current velocity. When the current velocity vanishes, only two-phase parameters among (, k,) are independent. Current wave models use the frequency-direction (,) as the independent phase variables.

WW3 uses the wavenumber-direction (k,) as the independent phase variables (Tolman, 1999). Without currents, the energy of a wave package is conserved. With currents the energy of a spectral component is no longer conserved (Longuet-Higgins and Stewart 1961), but the wave action spectrum, $N(k,\theta; \mathbf{x}, t)$ $F(k,\theta; \mathbf{x}, t)/$, is conserved (Whitham 1965; Bretherthon and Garrett 1968). In WWATCH, the balance equation is for the wave action spectrum.

4.2. Model Setting

WW3 has two types (mandatory and optional) of model switches for users to choose. Table 3 lists the model setting and optional switches for this study. For example, spatial and spectral grids are user-defined; the ultimate quickest propagation scheme is selected with the dispersion correction from Booij and Holthuijsen (1987); nonlinear interactions are included; and the source term parameterization follows Tolman and Chalikov (1996), Wittmann and Farra (1997), Tolman et al. (2002), and Chu and Cheng (2006) with consisting of four parts: wind input, nonlinear wave-wave interaction, dissipation, and wave-bottom interaction. The output of WWATCH consists of the traditional frequency-direction spectrum $F(\ ,\theta)$, which is calculated from $F(k,\ \theta)$ using Jacobean transformations. The NOAA global bathymetry dataset on a $1/12^{\circ} \times 1/12^{\circ}$ grid (ETOPO5) is used.

4.3. Discretization

The model is implemented for SCS (0^o to 25^o N, 105°-122°E) using realistic bathymetry data from the Naval Oceanographic Office DBDB5 database and a regularly spaced longitude-latitude grid with the grid spacing 0.25^o (i.e., $\Delta\ = \Delta\ = 0.25^o$). The wavenumber grid spacing is determined by the frequency intervals (total 25)

$$\sigma_{m+1} = X_{\sigma}\sigma_m,\ \text{m} = 0, 1, \ldots, 24, \tag{7}$$

with

$$X_{\sigma} = 1.1,\ \sigma_0 = 0.0418. \tag{8}$$

The wave direction ( ) grid spacing is 15^o (i.e., $\Delta\ = 15^o$).

Four time steps are used in WW3 to reach computational efficiency: (a) global time step (300 s) for the propagation of the entire solution, (b) spatial time step (300 s) representing the spatial propagation, (c) spectral time step (300 s) for intra-spectral propagation, and (d) source time step (100 s) for the source term integration.

4.4. Model Integration and Verification

WW3 is integrated from the JONSWAP wave spectra (Hasselmann et al. 1973, 1980) from 0000UTC 16 November to 1200UTC 25 November with the QTCWPM winds (Figure 7). Since TY Muifa entered the SCS as late as 19 November 2004, the model computation of the first three days, from 16 November to 18 November, could be considered as the 'spin up' period of WW3 model.

Due to lack of direct-measured platforms such as vessels or buoys during typhoon seasons in SCS, the T/P significant height (SWH) data are used for model verification. For TY Muifa (2004), the temporal covered QSCAT cycles are 448 (from 11 November 2004 to 21 November) and 449 (from 21 November and 01 December). There are 14 passes across the SCS area, which include 001, 012, 038, 051, 064, 077, 088, 114, 127, 140, 153, 164, 216, and 229. These passes have total 25 crossover points (Figure 8).

Figure 9 shows the comparison between WW3 result and T/P observation. The total number of H_s pairs is 38. The scattering diagram shows the clustering of points approximately located around the equal line. The histogram of the differences between model and observation shows Gaussian-type distribution. Examining the statistics, the bias of two datasets is 0.137 m with the root mean square error is 0.308 m, and the correlation coefficient is 0.895. The statistics suggests that the WW3 result and the T/P observation agreed well, and the numerical simulation during the period of TY Muifa is reasonably well.

5. Significant Wave Height

Figure 10 shows the daily evolution of significant wave height (H_s) in the SCS during the passage of TY Muifa. Here, the upper panels (Figure 10a-c) represent the period before TY Muifa

entering the SCS; the middle panels (Figure 10d-f) represent the period during TY Muifa passing through the SCS; and the lower panels (Figure 100g-i) represent the period after TY moving out from the SCS. Comparing to the evolution of QTCWPM wind field (Figure 7), close correlation is found between H_s and the typhoon winds. High H_s is with high wind speed and high waves appear to the right of the typhoon passage. The maximum H_s (16 m) occurs as TY Muifa reaches its lowest pressure in the SCS on 21 November.

Another high H_s occurs east of Luzon on 24 and 25 November (Figure 10h-i). Comparison between upper and lower panels of Figure 10 clearly shows the difference in monsoon-generated waves before TY Muifa arrival (Figure 10a-c) and after TY Muifa departure (Figure 10g-i). This indicates that the existing typhoon-generated wave field may affect the generation of new wind-wave field.

Figure 11a shows the horizontal distributions of WW3 generated maximum H_s and maximum wind speed during TY Muifa passage from 17 to 25 November. The core of the maximum wind speed is symmetric along the track of the TY Muifa passage (Figure 11b). However, the core of the maximum H_s is asymmetric in width and in value along the track of TY Muifa (Figure 11a) with higher H_s in the right side of the track than the left side.

TY Muifa has its lowest pressure at L-II (11.6^{o}N, 114.4^{o}E) at 1800UTC on 21 November. Figure 12 shows the horizontal distribution of H_s at L-II with the typhoon translation axis being rotated towards north and RMW of 14.0 km. The high values of H_s are in the right forward quadrant with the maximum H_s of 16 m slightly outside of RMW from the typhoon center. This consists with earlier studies (Moon et al. 2003) that the wave generation on the typhoon center has an asymmetric distribution in four quadrants.

6. Directional Wave Spectra

Figure 13 shows the daily evolution of directional wave spectra at L-II. The arrow indicates the wind speed and direction at each moment. The winds (7.8 m/s) blow from northeast (45° from the north) before 1800UTC on 20 November and after 1800UTC on 23 November, showing the dominant winter monsoon. In these two periods, a set of low-frequency waves exists and aligns with the wind in a slight leftward angle. Conversely, from 1800UTC on 20 November to 1800UTC on 23 November, wave direction and frequency change rapidly. Furthermore, after the departure of TY Muifa, evident wave packet still remains in the direction from 30° to 70°.

Variation of the directional wave spectra during TY Muifa passage is represented using 6-hourly spectral evolution (Figure 14) from 1800UTC on 20 November to 1800UTC on 22 November. While the winds increase and turn counterclockwise as TY Muifa passing by, the waves are generated along with the turning wind directions. As the typhoon located right on L-II at 1800UTC on 21 November, the wind speed significantly decreases and the wind vector shifts to the opposite direction. A wide range of waves are generated with monsoon dominated swell in the southwestward direction, and that, as typhoon wind changes rapidly in speed and direction, a pair of wave packets are generated at the time of typhoon arrival (Figure 14e). These typhoon-generated waves, especially in the opposite direction to monsoon winds (i.e., the northeastward direction) decay fast but still exist four days after the typhoon departure.

7. Effect of Typhoon Translation Speed

Figure 15 shows 6-hourly evolutions of H_s at the typhoon center for all four locations (L-I to L-IV). In order to investigate the effect of typhoon translation speed, all the H_s fields have been

rotated with the typhoon translation axis pointing toward north. Comparison of the H_s fields between L-I and L-III leads to the effects of typhoon translation speed on the wave characteristics. The maximum H_s is moving faster at L-I than at L-III. The value of maximum H_s at L-I increases as the typhoon low pressure decreases. The highest H_s is located slightly outside RMW from the typhoon center in the right forward quadrant, and that, the higher typhoon translation speed the larger the angle is between the highest H_s and the eastward direction.

Four-way locations are selected around the TY Muifa center with RMW away to investigate the effect of translation speed on the directional wave spectra: forward location (F), backward location (B), rightward location (R), and leftward location (L) (see up-left panel of Figure 16 to Figure 19). The typhoon center is indicated by 'C'. The dashed curves are circles with RMW from the typhoon centers. The hollow arrow indicates the typhoon's translation velocity vector. The solid arrow is the wind vector at each location. Consistent with the previous study (Moon et al. 2003), the wave spectra in the forward location (F) and rightward location (R) show the generation of high-frequency waves aligning with the wind direction due to resonant effects. But the wave spectra in the leftward location (L) and backward location (B) have more complicated structures.

For the same typhoon intensity (L-I and L-III), the directional wave spectra at the typhoon center (location-C) is more asymmetrical for the faster translation speed (Figure 16) than for the slower translation speed (Figure 18). High wave energy centers occur in both forward and backward directions for the slower translation speed [Figure 18(C)] but not for the faster translation speed [Figure 16(C)].

8. Effect of Typhoon Intensity

Typhoon has the same translation speed but different intensity at L-II and L-IV. Comparison of H_s and directional wave spectra between L-II and L-IV leads to the effect of typhoon intensity. Figure 15 shows that the maximum H_s is at least 5 m larger and located closer to the typhoon center at L-II than at L-IV. This is because the typhoon is stronger with smaller R_m at L-II than at L-IV. As the typhoon translation speed increases significantly at L-IV (7.29 m/s), the shape of H_s contours becomes elliptic.

The directional wave spectra at the typhoon center clearly show the following features. The waves are generated in both frontward and backward directions for higher typhoon intensity [L-II, Figure 17(C)], but only in the frontward direction for lower typhoon intensity [L-IV, Figure 19(C)]. Among the four locations around the typhoon center, the directional wave spectra are very different at locations (F, R, and L) but less different at location B between L-II and L-IV. At locations (F, R, and L), two wave packets are generated in both upwind and downwind directions for high typhoon intensity (Figure 17), but only one wave packet is generated in downwind direction for low typhoon intensity (Figure 19). The difference between L-II and L-IV (comparing Figure 17 with Figure 19) is much larger than the difference between L-I and L-III (comparing Figure 16 with Figure 18). This indicates that the effect of typhoon intensity is much larger than the effect of typhoon translation speed on the SCS wave characteristics.

9. Conclusions

This study investigates the South China Sea wave characteristics using WW3 with winter typhoon forcing. The model was forced by high resolution wind field, which was obtained from the QuikSCAT data combined with the tropical cyclone wind profile model. The WW3 model was

evaluated using the TOPEX/Poseidon altimetry observation during the period of Typhoon Muifa (2004).

Along the typhoon translation track, the core of the maximum significant wave height (H_s) was asymmetric with higher H_s and wider core in the right side than the left side. The maximum H_s was about 16 m located at minimum typhoon lowest pressure center. At a single position, the maximum H_s was always in the right-front quadrant of the typhoon center and located slightly outside RMW.

The waves were generated in both frontward and backward directions for higher typhoon intensity, but only in the frontward direction for lower typhoon intensity. When the typhoon intensity was reduced (from L-II to L-IV), the directional wave spectra were very different at the frontward, rightward, and leftward locations. Two wave packets were generated in both upwind and downwind directions for high typhoon intensity, but only one wave packet was generated in downwind direction for low typhoon intensity. However, the directional wave spectra were less different at the backward location. For the typhoon-generated waves in the South China Sea, the factors affecting its wave characteristics with their importance from large to small are listed as follows: typhoon intensity, distance and direction from typhoon center, the typhoon translation speed, monsoon, and topography.

As the typhoon passed by, wind speed and direction changed rapidly. Stronger intensity with slower translation speed usually generated a pair of wave packets. The typhoon-generated waves can propagate across the South China Sea farther than 1000 km in distance. Along the wave propagation direction, the obstructions of coastline and small islands generated the wave shadow zones. This feature implies that the SCS, a semi-close marginal sea, can be considered as an

independent wave system from nearby oceans except the energy transform through the Luzon Strait, which is deep to 1800 m. The Sulu Sea, which separated by the Palawan Island, can be seen as a different wave system from the SCS.

Acknowledgements

The authors wish to thank Dr. Tolman at the National Weather Service for providing the Wavewatch-III model, the NOAA-CIRES Climate Diagnostics Center for providing NCEP Reanalysis data, and NASA/JPL for providing TOPEX/POSEIDON data. This work was jointly funded by the Naval Oceanographic Office, and the Naval Postgraduate School.

References

Barber, N. F., F. Ursell, 1948: The generation and propagation of ocean waves and swell. Part-I. Wave periods and velocities. *Phil. Trans. Royal Soc. London., Series A., Math. Phys. Sci.*, **240**, 527-560.

Carr, L. E. III, and R. L. Elsberry, 1997: Models of tropical cyclone wind distribution and beta-effect propagation for application to tropical cyclone track forecasting. *Mon. Weather Rev.*, **125**, 3190-3209.

Chu, P. C., J. M. Veneziano, C. W. Fan, M. J. Carron, and W. T. Liu, 2000: Response of the South China Sea to tropical cyclone Ernie 1996. *J. Geophys. Res.-Oceans,* **105**, 13991-14009.

Chu, P. C., Y. Q. Qi, Y. C. Chen, P. Shi, and Q. W. Mao, 2004: South China Sea wind-wave characteristics. Part I: Validation of Wavewatch-III using TOPEX/Poseidon data. *J. Atmos. Oceanic Technol.,* **21**, 1718-1733.

Chu, P.C., and K.F. Cheng, 2006: Effect of wave boundary layer on sea-to-air dimethylsulfide transfer velocity during typhoon passage. J. Marine Syst., in press.

Hasselmann, D. E., M. Dunckel, and J. A. Ewing, 1980: Directional wave spectra observed during JONSWAP 1973. *J. Phys. Oceanogr.,* **10**, 1264-1280.

Hsu, Y.L., W.E. Roger, and J.D. Dykes, 2002: WAM performance in the Gulf of Mexico with COAMPS wind. 7th International Workshop on Wave Hindcast and Forecast, Banff, Alberta, Canada, October 21-25, 2002, 9 pages (in CD Rom).

Holt, B., A. K. Liu, D. W. Wang, A. Gnanadesikan, and H. S. Chen, 1998: Tracking storm-generated waves in the northeast Pacific Ocean with ERS-1 synthetic aperture radar imagery and buoys. *J. Geophys .Res.- Oceans,* **103**, 7917-7929.

Hwang, P. A., and Wang, D. W., 2001: Directional distributions and mean square slopes in the equilibrium and saturation ranges of the wave spectrum. *J. Phys. Oceanogr.*, **31**, 1346-1360.

JTWC, 2005: 2004 Annual Tropical Cyclone Report. [Available online at http://www.npmoc.navy.mil/jtwc/atcr/2004atcr/].

Moon, I., I. Ginis, T. Hara, H. L. Tolman, C. W. Wright, and E. J. Walsh, 2003: Numerical simulation of sea surface directional wave spectra under hurricane wind forcing. *J. Phys. Oceanogr.*, **33**, 1680-1706.

Tolman, H. L., D. Chalikov, 1996: Source terms in a third-generation wind wave model. *J. Phys. Oceanogr.*, **26**, 2497-2518.

Tolman, H. L., 1999: User manual and system documentation of WAVEWATCH-III version 1.18. Vol. NOAA/NCEP Technical Note 166, US Department of Commerce, 110 pp.

Tolman, H. L., B. Balasubramaniyan, L. D. Burroughs, D. V. Chalikov, Y. Y. Chao, H. S. Chen, and V. M. Gerald, 2002: Development and implementation of wind-generated ocean surface wave models at NCEP. *Weather Forecast.*, **17**, 311-333.

Walsh, E. J., D. W. Hancock III, D. E. Hines, R. N. Swift, and J. F. Scott, 1989: An observation of the directional wave spectrum evolution from shoreline to fully developed. *J. Phys. Oceanogr.*, **19**, 670-690.

Wittmann, P. A., and P.D. Farra, 1997: Global, regional and coastal wave prediction. Marine Tech. J., 31 (1): 76-82.

Wright, C. W., E. J. Walsh, D. Vandemark, W. B. Krabill, A. W. Garcia, S. H. Houston, M. D. Powell, P. G. Black, and F. D. Marks, 2001: Hurricane directional wave spectrum spatial variation in the open ocean. *J.Phys.Oceanogr.*, **31**, 2472-2488.

Wyatt, L. R., 1995: The Effect of Fetch on the Directional spectrum of Celtic Sea storm waves. *J. Phys. Oceanogr.*, **25**, 1550-1559.

Table Captions

Table 1. The Best Track Record of TY Muifa (2004) during 0000UTC 16 November to 0600UTC 25 November 2004 (From JTWC 2005).

Table 2. Translation speed (calculated from Table 1) and estimated radius parameters for TY Muifa (2004).

Table 3. WW3 model setting for this study.

Figure Captions

Fig. 1. Geography of the South China Sea.

Fig. 2. The best track passage of TY Muifa (2004) (from JTWC 2005).

Fig. 3. Several parameters along the passage of TY Muifa (2004): (a) translation speed, (b) lowest pressure, (c) maximum wind speed, and (d) the water depth. Four lines indicate designed locations of typhoon centers.

Fig 4. The location of 4 designed typhoon centers. Dotted line indicates the water depth of 100 m (near shore) and 2000 m (open ocean).

Fig 5. Daily QSCAT wind vector fields on 17-25 November 2004.

Fig. 6. Temporally mean QSCAT wind vector field from 0000UTC on 16 November to 0600UTC on 25 November 2004.

Fig. 7. Daily QTCWPM wind vector fields on 17-25 November 2004.

Fig 8. TOPEX/Poseidon crossover points in the SCS.

Fig. 9. Comparison of significant wave height between model (WW3) simulated and observed

(TOPEX/POSEIDON) on all crossover points during the passage of TY Muifa (2004): (a) scatter diagram, and (b) histogram distribution of difference between modeled and observed values.

Fig 10. Daily evolution of H_s in the SCS during the passage of TY Muifa (2004).

Fig. 11. Horizontal l distributions during the passage of TY Muifa (2004): (a) maximum H_s calculated using WW3, and (b) maximum QTCWPM wind speeds.

Fig 12. Horizontal distribution of in the SCS at 1800UT on 21 November when the lowest pressure center of TY Muifa is located at (11.6^{o}N, 114.4^{o}E). The estimated maximum wind radius is about 14.0 km. The translation direction (hollow arrow) is rotated to northward.

Fig 13. Daily evolution of directional wave spectra with QTCWPM winds on L-II (11.6^{o}N and 114.4^{o}E). TY Muifa was at this location at 1800UTC on 21 November. The arrow presents QTCWPM wind speed and direction.

Fig 14. Six-hourly evolution of directional wave spectra with QTCWPM winds on L-II (11.6^{o}N and 114.4^{o}E) from 1800UTC on 20 November to 1800UTC on 21 November. TY Muifa was at this location at 1800UTC on 21 November. The arrow presents QTCWPM wind speed and direction.

Fig. 15. Six-hourly evolutions of H_s at four locations (from vertical direction): (a) before typhoon arrivals (left column), (b) typhoon right on (central column), and (c) after typhoon departures (right

column). The translation directions are rotated to northward.

Figure 16. Wave characteristics at L-1 (11.9^{o}N, 117.2^{o}E, 0000UTC on 21 November): horizontal distribution of H_S and directional wave spectra at center (C) and four-way locations around the TY Muifa center with RMW away forward location (F), backward location (B), rightward location (R), and leftward location (L).

Figure 17. Wave characteristics at L-II (11.6^{o}N, 114.4^{o}E, 1800UTC on 21 November): horizontal distribution of H_S and directional wave spectra at center (C) and four-way locations around the TY Muifa center with RMW away forward location (F), backward location (B), rightward location (R), and leftward location (L).

Figure 18. Wave characteristics at L-1II (10.5^{o}N, 112.1^{o}E, 1800UTC on 22 November): horizontal distribution of H_S and directional wave spectra at center (C) and four-way locations around the TY Muifa center with RMW away forward location (F), backward location (B), rightward location (R), and leftward location (L).

Figure 19. Wave characteristics at L-1II (8.8^{o}N, 108.8^{o}E, 0600UTC on 24 November): horizontal distribution of H_S and directional wave spectra at center (C) and four-way locations around the TY Muifa center with RMW away forward location (F), backward location (B), rightward location (R), and leftward location (L).

Table 1. The Best Track Record of TY Muifa (2004) during 0000UTC 16 November to 0600UTC 25 November 2004 (From JTWC 2005).

Date	Time	Lat (N)	Long (E)	Type	Pressure (μPa)	V_{max} (m/sec)	R18 (km)	R26 (km)	R33 (km)
11/16/2004	00:00	14.5	125.7	TS	994	20.6	148	--	--
11/16/2004	06:00	14.5	124.9	TS	991	23.1	183	--	--
11/16/2004	12:00	14.5	124.2	TS	984	28.3	183	56	--
11/16/2004	18:00	14.4	123.6	TS	984	28.3	174	56	--
11/17/2004	00:00	14.6	123.6	TS	980	30.9	219	70	--
11/17/2004	06:00	14.8	123.6	TY	976	33.4	213	74	28
11/17/2004	12:00	15.2	123.8	TY	967	38.6	213	74	28
11/17/2004	18:00	15.5	123.8	TY	954	46.3	174	74	46
11/18/2004	00:00	15.7	123.8	TY	938	54	156	65	46
11/18/2004	06:00	15.9	123.9	TY	927	59.2	167	65	46
11/18/2004	12:00	15.9	124.2	TY	927	59.2	170	70	46
11/18/2004	18:00	15.7	124.4	TY	938	54	133	59	41
11/19/2004	00:00	15.2	124.2	TY	938	54	109	59	41
11/19/2004	06:00	14.7	124.1	TY	954	46.3	139	59	41
11/19/2004	12:00	14.2	123.7	TY	958	43.7	144	59	41
11/19/2004	18:00	13.7	122.8	TY	963	41.2	131	56	37
11/20/2004	00:00	12.8	121.6	TY	967	38.6	137	56	37
11/20/2004	06:00	12.5	120.3	TY	976	33.4	137	56	--
11/20/2004	12:00	12.3	119.3	TS	980	30.9	115	56	--
11/20/2004	18:00	12.2	118.3	TY	976	33.4	115	56	--
11/21/2004	00:00	11.9	117.2	TY	976	33.4	128	56	--
11/21/2004	06:00	11.9	116.1	TY	972	36	152	56	28
11/21/2004	12:00	11.8	115.2	TY	963	41.2	152	65	37
11/21/2004	18:00	11.6	114.4	TY	954	46.3	152	65	37
11/22/2004	00:00	11.4	113.6	TY	958	43.7	152	65	37
11/22/2004	06:00	11.1	113.1	TY	958	43.7	126	59	33
11/22/2004	12:00	10.8	112.6	TY	967	38.6	120	52	33
11/22/2004	18:00	10.5	112.1	TY	976	33.4	120	52	33
11/23/2004	00:00	10.1	111.7	TY	976	33.4	120	52	--
11/23/2004	06:00	9.9	111.1	TY	976	33.4	111	56	--
11/23/2004	12:00	9.6	110.6	TS	980	30.9	109	48	--
11/23/2004	18:00	9.3	110.2	TS	984	28.3	107	44	--
11/24/2004	00:00	9.1	109.7	TS	984	28.3	107	44	--
11/24/2004	06:00	8.8	108.8	TS	987	25.7	120	52	--
11/24/2004	12:00	8.5	107.4	TS	994	20.6	102	--	--
11/24/2004	18:00	8.3	105.7	TS	994	20.6	93	--	--
11/25/2004	00:00	8.7	103.6	TS	994	20.6	93	--	--
11/25/2004	06:00	8.7	101.7	TS	997	18	96	--	--

Table 2. Translation speed (calculated from Table 1) and estimated radius parameters for TY Muifa (2004).

Date	Time	Position		TS (m/s)	V_{max} (m/s)	Wind Profile Radius			Determined Parameters		
		Lat (N)	Long (E)			R_{18} (km)	R_{26} (km)	R_{33} (km)	R_s (km)	R_{max} (km)	R_0 (km)
11/16	00:00	14.5	125.7	3.99	20.6	148	--	--	54.8	89.3	630
11/16	06:00	14.5	124.9	3.99	23.1	183	--	--	54.2	88.9	680
11/16	12:00	14.5	124.2	3.49	28.3	183	56	--	43.2	71.8	678
11/16	18:00	14.4	123.6	3.04	28.3	174	56	--	32.6	54.8	666
11/17	00:00	14.6	123.6	1.03	30.9	219	70	--	36.6	61.5	725
11/17	06:00	14.8	123.6	1.03	33.4	213	74	28	18.9	32.2	623
11/17	12:00	15.2	123.8	2.29	38.6	213	74	28	23.8	40.5	725
11/17	18:00	15.5	123.8	1.54	46.3	174	74	46	10.4	17.9	638
11/18	00:00	15.7	123.8	1.03	54.0	156	65	46	8.1	14.0	655
11/18	06:00	15.9	123.9	1.14	59.2	167	65	46	8.1	14.0	693
11/18	12:00	15.9	124.2	1.49	59.2	170	70	46	8.1	14.0	693
11/18	18:00	15.7	124.4	1.43	54.0	133	59	41	8.1	14.0	655
11/19	00:00	15.2	124.2	2.76	54.0	109	59	41	8.1	14.0	670
11/19	06:00	14.7	124.1	2.62	46.3	139	59	41	8.1	14.0	615
11/19	12:00	14.2	123.7	3.26	43.7	144	59	41	9.3	16.0	631
11/19	18:00	13.7	122.8	5.18	41.2	131	56	37	9.8	16.9	629
11/20	00:00	12.8	121.6	7.59	38.6	137	56	37	10.6	18.2	661
11/20	06:00	12.5	120.3	6.71	33.4	137	56	--	15.7	26.9	663
11/20	12:00	12.3	119.3	5.13	30.9	115	56	--	16.8	28.7	646
11/20	18:00	12.2	118.3	5.06	33.4	115	56	--	13.7	23.5	648
11/21	00:00	11.9	117.2	5.75	33.4	128	56	--	14.2	24.4	667
11/21	06:00	11.9	116.1	5.54	36.0	152	56	28	14.7	25.2	710
11/21	12:00	11.8	115.2	4.56	41.2	152	65	37	10.6	18.3	714
11/21	18:00	11.6	114.4	4.16	46.3	152	65	37	8.1	14.0	725
11/22	00:00	11.4	113.6	4.16	43.7	152	65	37	9.1	15.7	729
11/22	06:00	11.1	113.1	2.96	43.7	126	59	33	8.1	14.0	718
11/22	12:00	10.8	112.6	2.96	38.6	120	52	33	10.4	17.9	721
11/22	18:00	10.5	112.1	2.96	33.4	120	52	33	16.7	28.6	763
11/23	00:00	10.1	111.7	2.89	33.4	120	52	--	12.8	22.0	726
11/23	06:00	9.9	111.1	3.21	33.4	111	56	--	11.7	20.1	716
11/23	12:00	9.6	110.6	2.97	30.9	109	48	--	14.3	24.6	733
11/23	18:00	9.3	110.2	2.55	28.3	107	44	--	16.7	28.6	738
11/24	00:00	9.1	109.7	2.74	28.3	107	44	--	16.7	28.6	749
11/24	06:00	8.8	108.8	4.83	25.7	120	52	--	23.7	40.4	795
11/24	12:00	8.5	107.4	7.29	20.6	102	--	--	33.7	56.9	775
11/24	18:00	8.3	105.7	8.72	20.6	93	--	--	30.4	51.5	763
11/25	00:00	8.7	103.6	10.89	20.6	93	--	--	30.5	51.6	739
11/25	06:00	8.7	101.7	9.67	18.0	96	--	--	47.3	78.8	772

Table 3. WW3 model setting for this study.

Switch Parameters	Characteristics
DUM	Dummy to be used if WWATCH is to be installed on previously untried hardware
LRB8	8 byte words
SHRD	Shared memory model, no message passing
SEED	Seeding of high-frequency energy
GRD1	Settings directly hardwired to user-defined spatial grids (spherical coordinate with 0.25^{o} grids)
SP1	User-defined spectral grids.
PR2	Ultimate quickest propagation scheme with Booij and Holthuijsen (1987) dispersion correction
ST2	Tolman and Chalikov (1996) source term package
STAB2	Enable stability correction for Tolman and Chalikov (1996) source term package
NL1	Nonlinear interaction (DIA)
BT1	JONSWAP bottom friction formulation
WIND2	Approximately quadratic interpolation
CUR2	Approximately quadratic interpolation
o1	Output of boundary points in grid preprocessor
o2	Output of the grid point status map in grid preprocessor
o2a	Generation of land-sea mask file mask.WW3 in grid preprocessor
o3	Additional output in loop over fields in field preprocessor
o4	Print plot of normalized 1-D energy spectrum in initial conditions program
o5	2-D energy spectrum
o6	Spatial distribution of wave heights (not adapted for distributed memory)
o7	Echo input data for homogeneous fields in generic shell

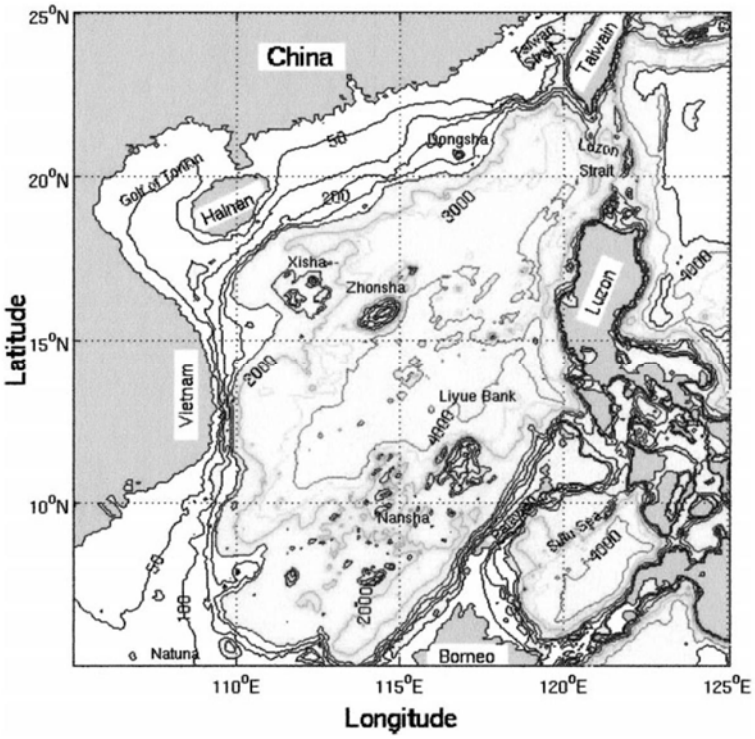

Fig. 1. Geography of the South China Sea.

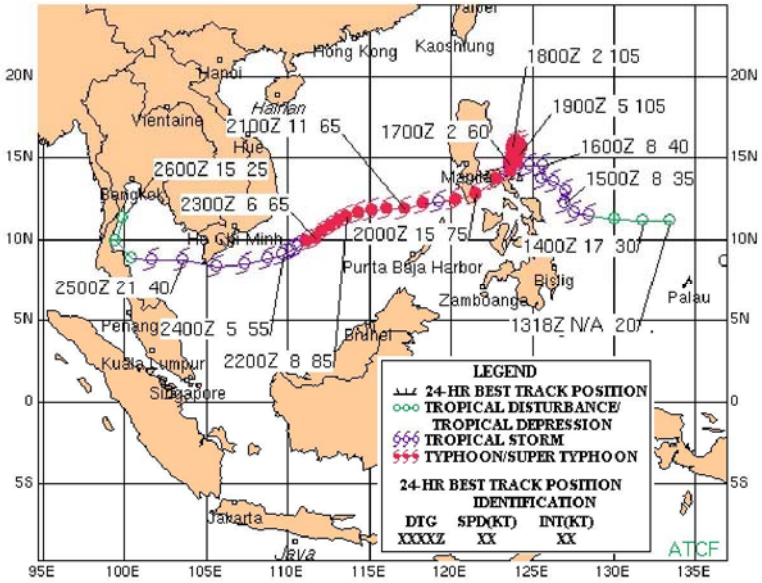

Fig. 2. The best track passage of TY Muifa (2004) (from JTWC 2005).

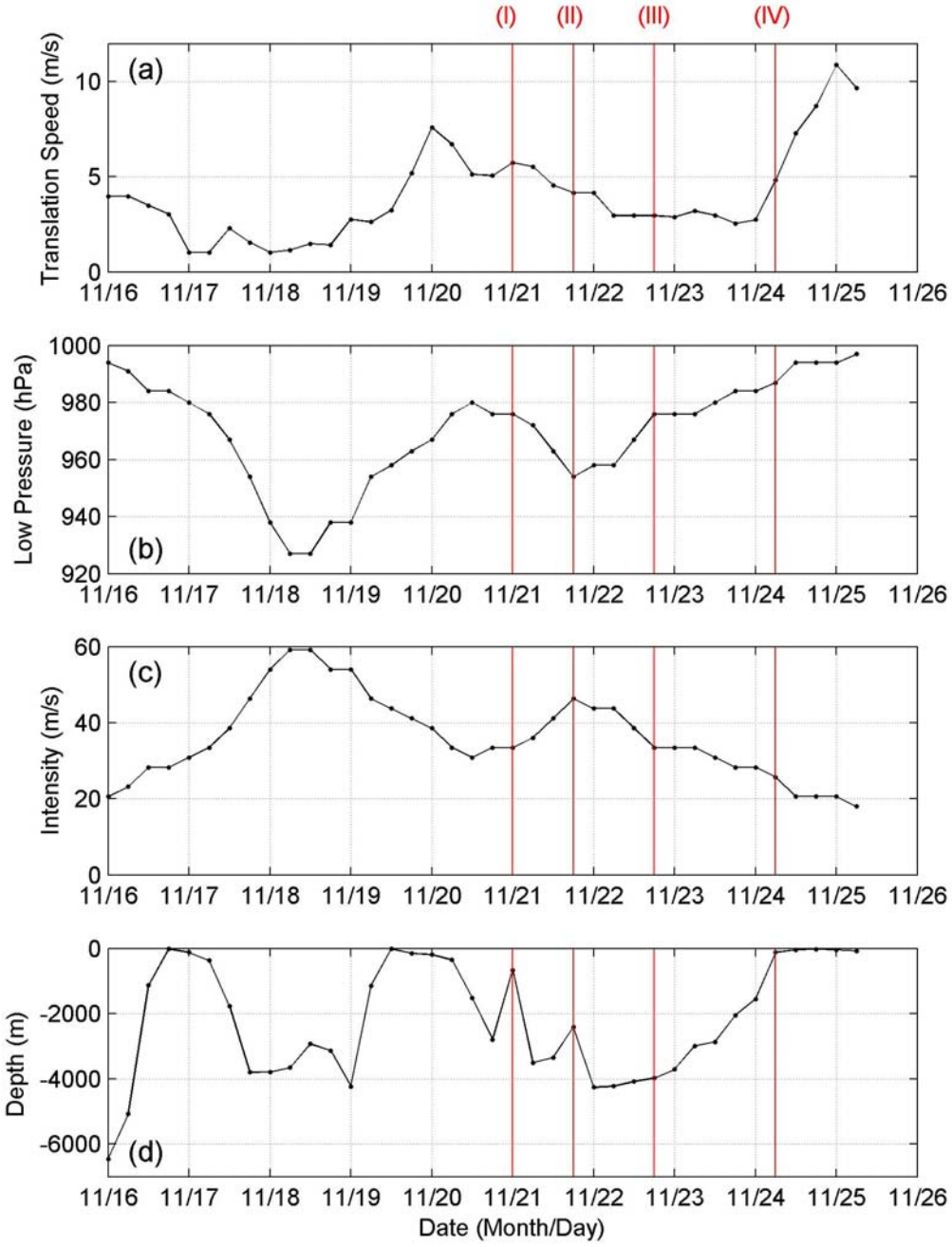

Fig. 3. Several parameters along the passage of TY Muifa (2004): (a) translation speed, (b) lowest pressure, (c) maximum wind speed, and (d) the water depth. Four lines indicate designed locations of typhoon centers.

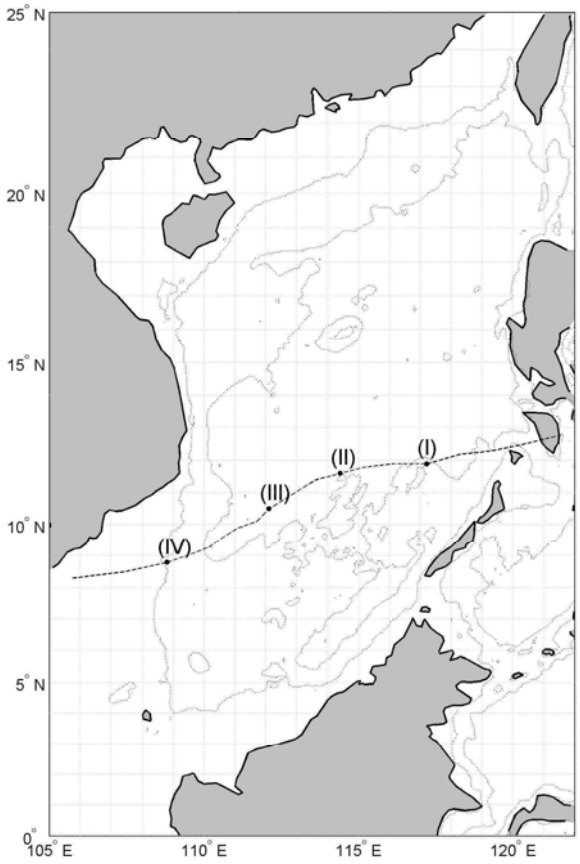

Fig 4. The location of 4 designed typhoon centers. Dotted line indicates the water depth of 100 m (near shore) and 2000 m (open ocean).

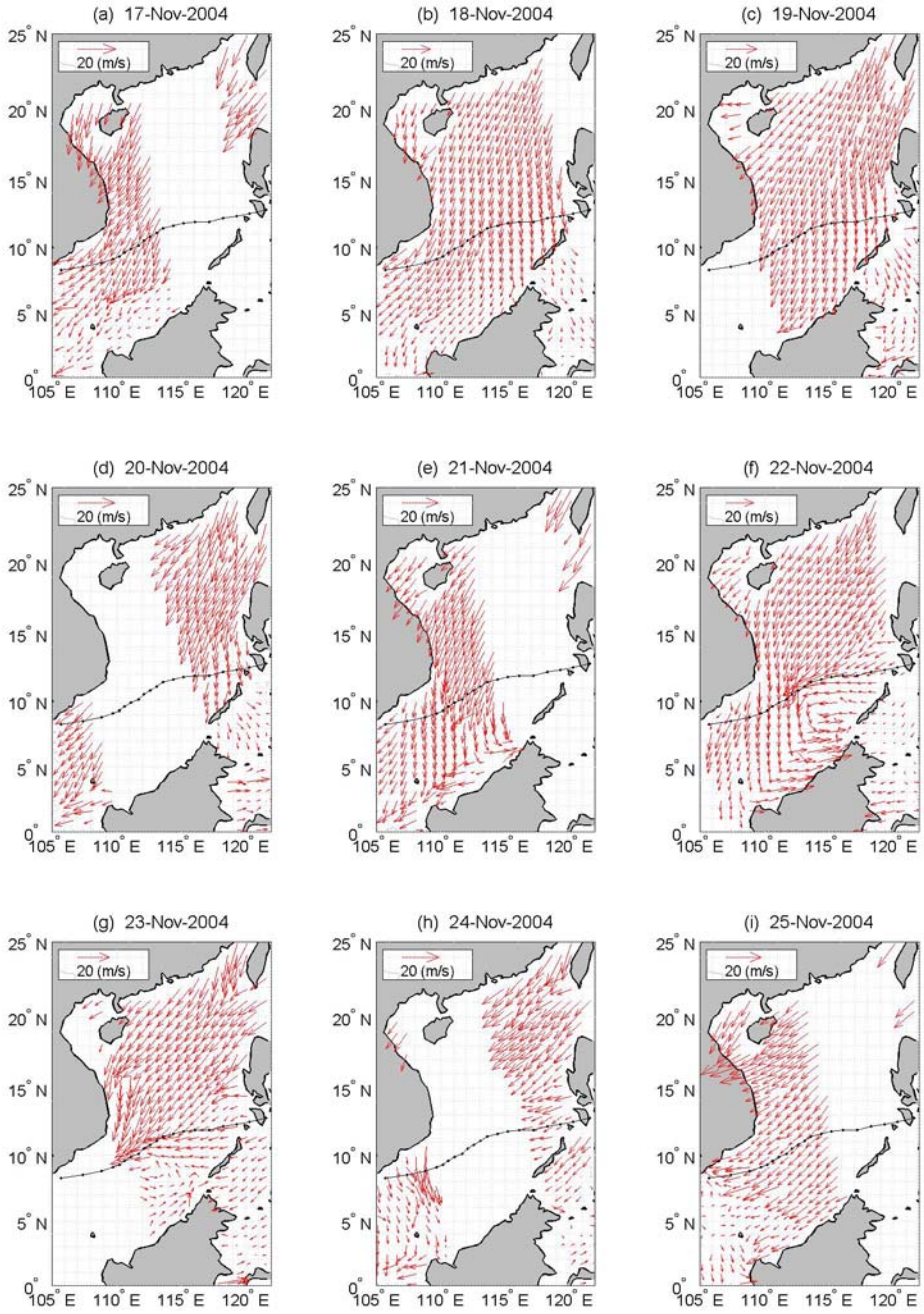

Fig 5. Daily QSCAT wind vector fields on 17-25 November 2004.

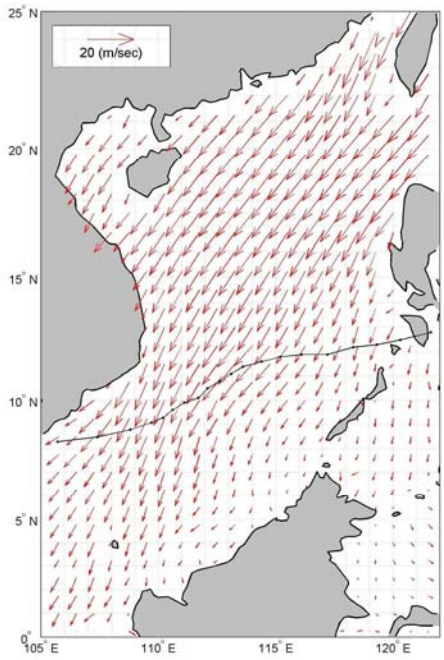

Fig. 6. Temporally mean QSCAT wind vector field from 0000UTC on 16 November to 0600UTC on 25 November 2004.

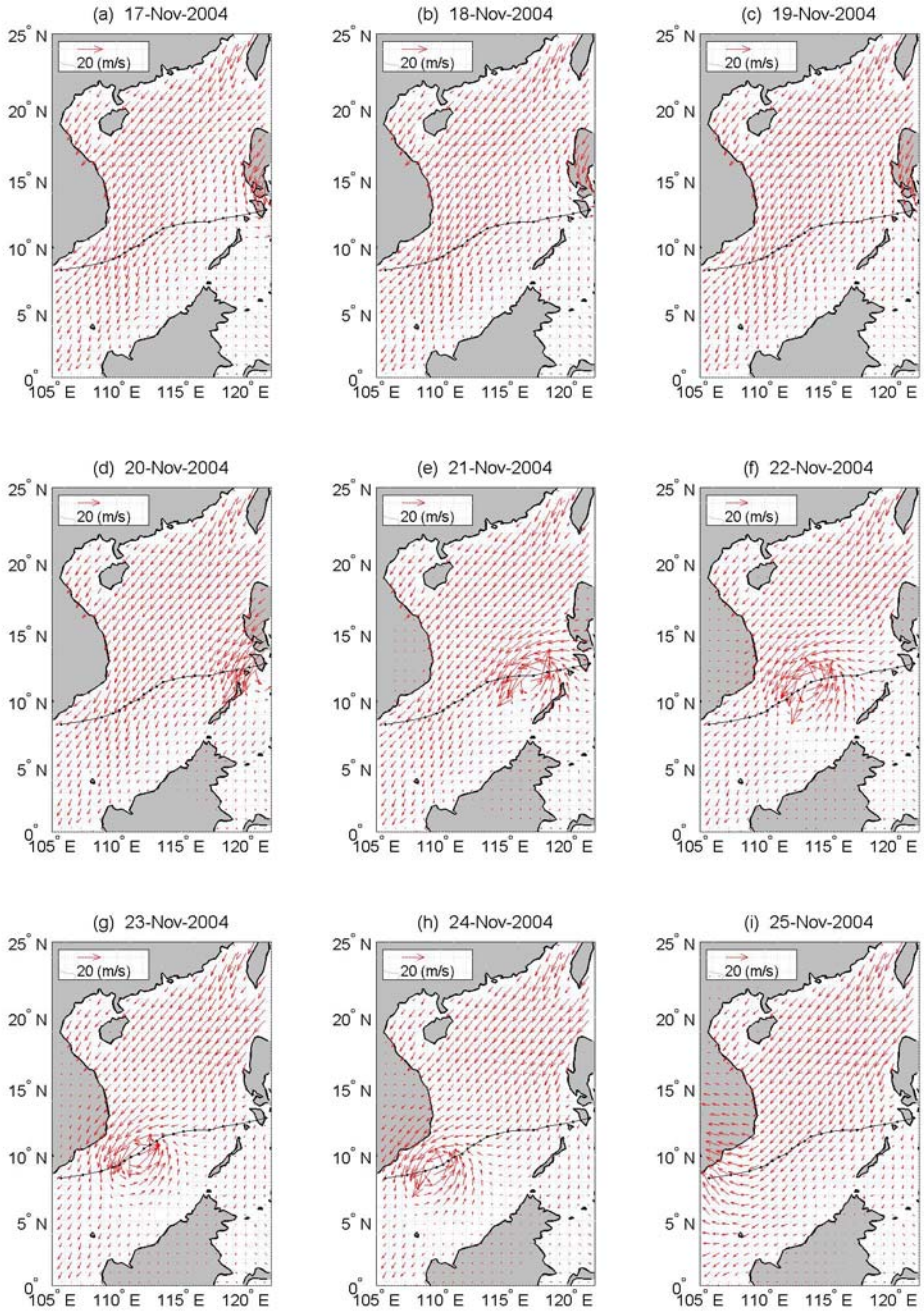

Fig. 7. Daily QTCWPM wind vector fields on 17-25 November 2004.

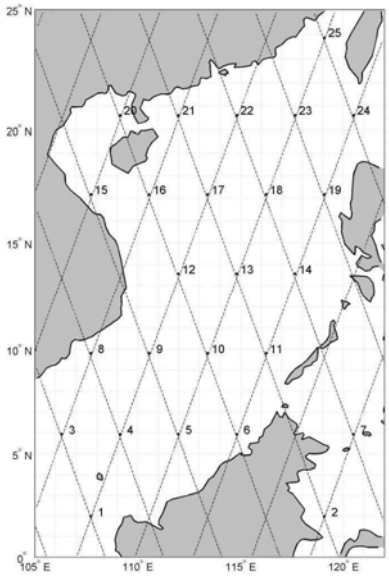

Fig 8. TOPEX/Poseidon crossover points in the SCS.

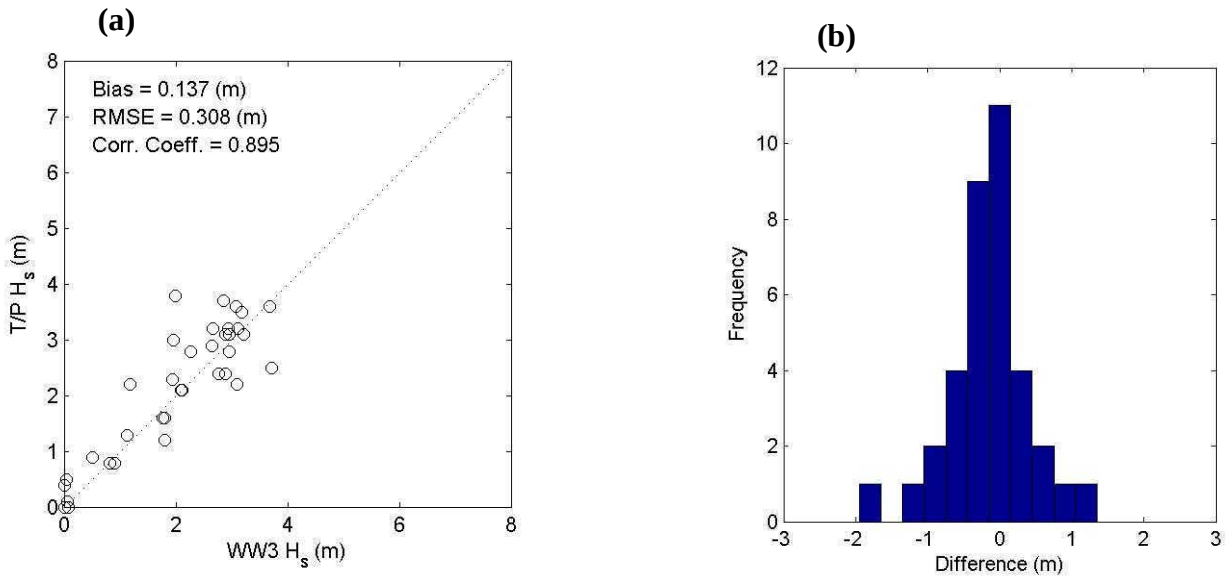

Fig. 9. Comparison of significant wave height between model (WW3) simulated and observed (TOPEX/POSEIDON) on all crossover points during the passage of TY Muifa (2004): (a) scatter diagram, and (b) histogram distribution of difference between modeled and observed values.

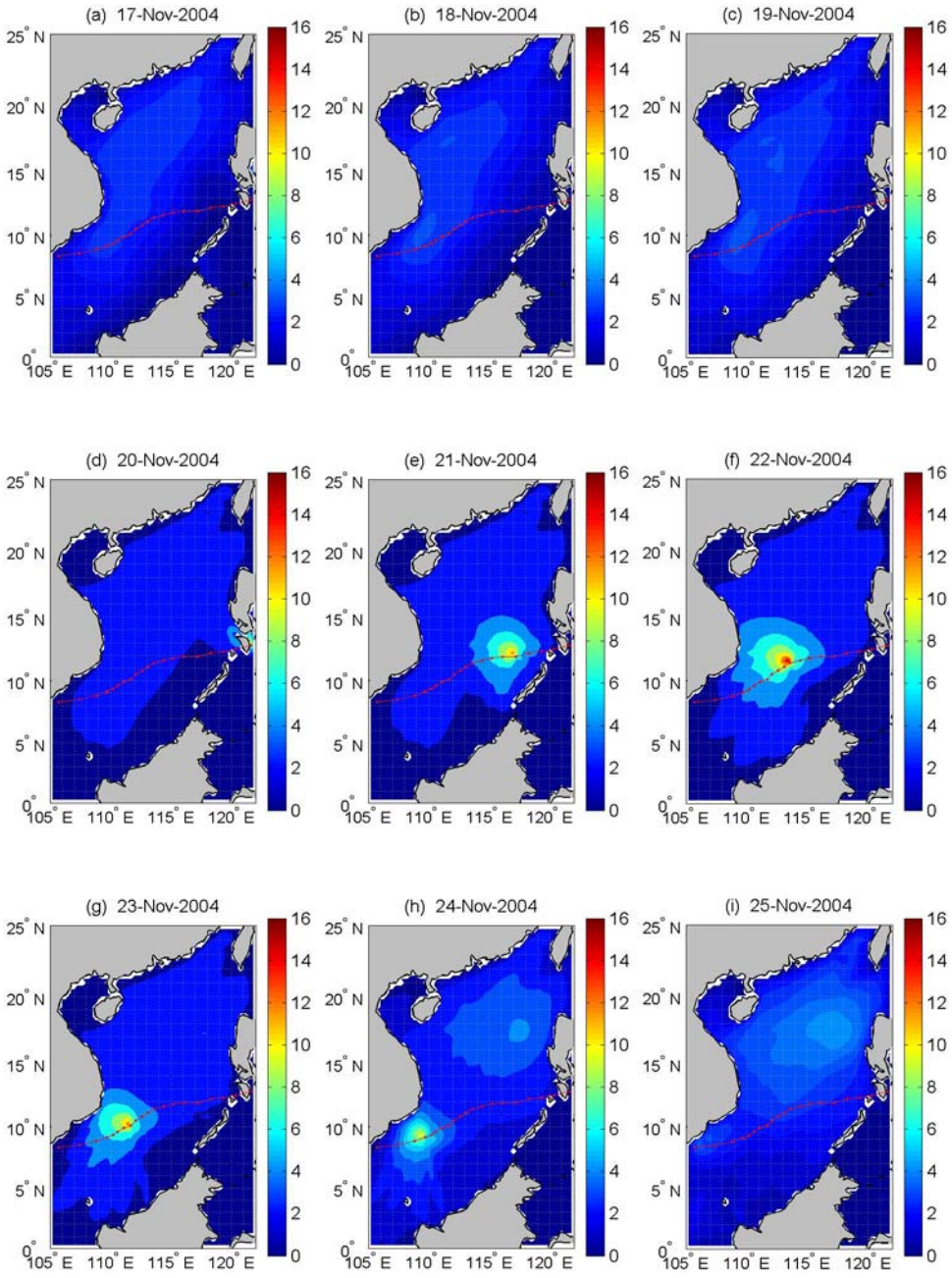

Fig 10. Daily evolution of H_s in the SCS during the passage of TY Muifa (2004).

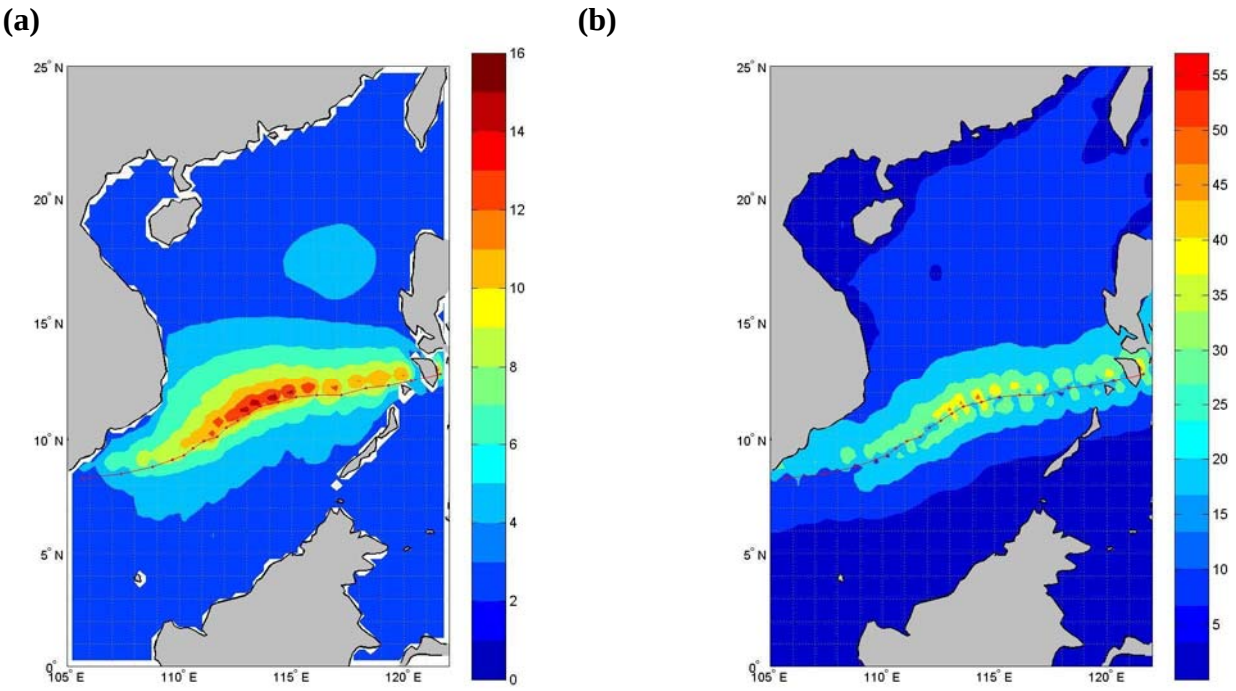

Fig. 11. Horizontal l distributions during the passage of TY Muifa (2004): (a) maximum H_s calculated using WW3, and (b) maximum QTCWPM wind speeds.

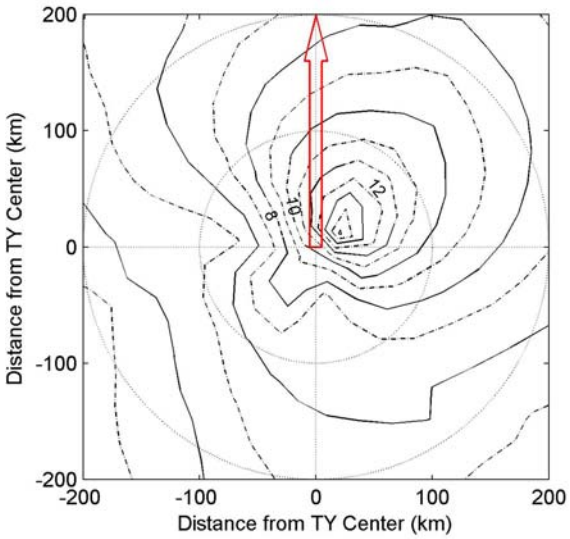

Fig 12. Horizontal distribution of in the SCS at 1800UT on 21 November when the lowest pressure center of TY Muifa is located at (11.6^{o}N, 114.4^{o}E). The estimated maximum wind radius is about 14.0 km. The translation direction (hollow arrow) is rotated to northward.

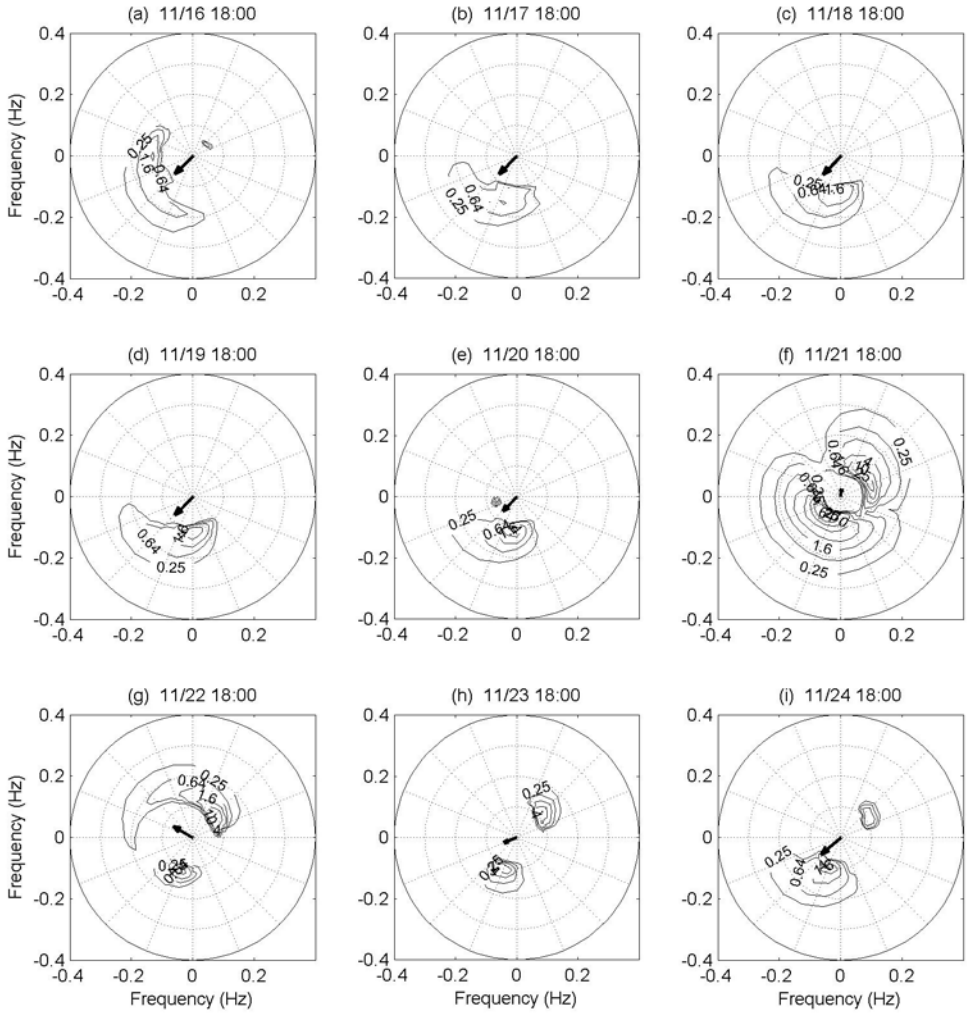

Fig 13. Daily evolution of directional wave spectra with QTCWPM winds on L-II (11.6^{o}N and 114.4^{o}E). TY Muifa was at this location at 1800UTC on 21 November. The arrow presents QTCWPM wind speed and direction.

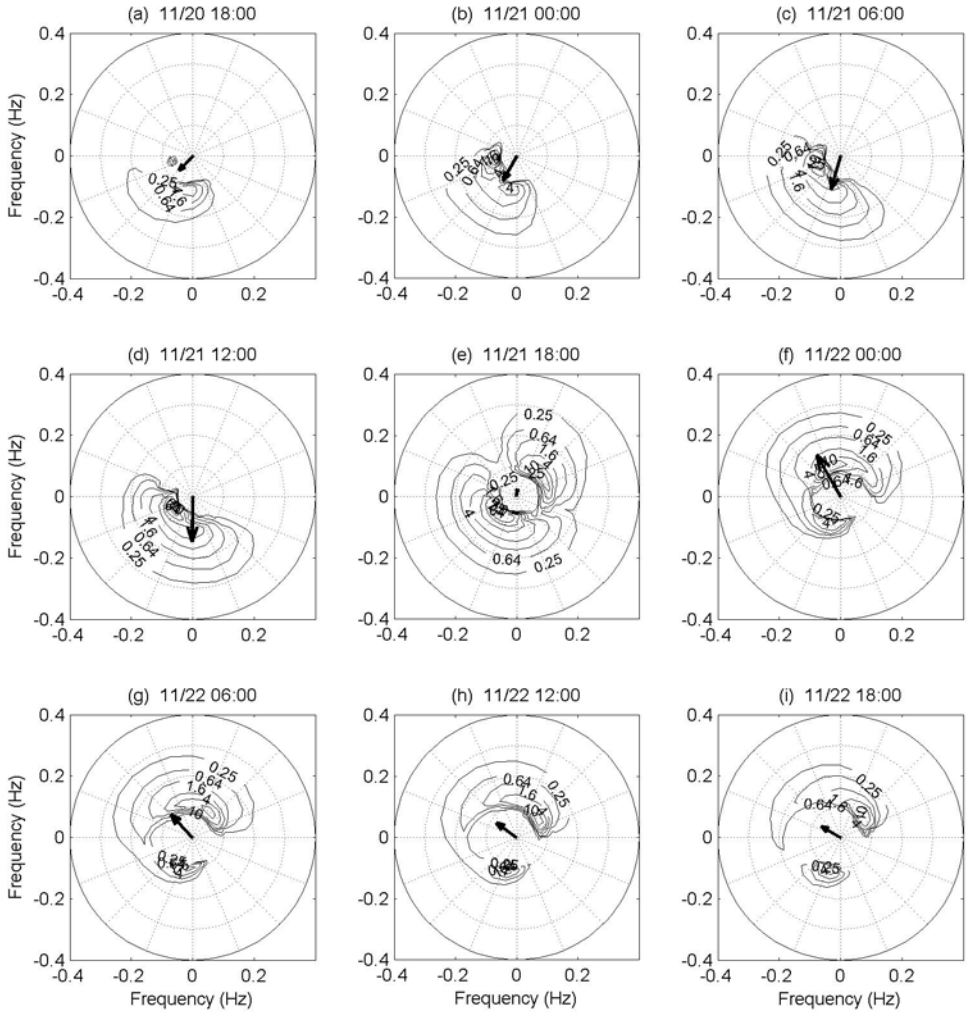

Fig 14. Six-hourly evolution of directional wave spectra with QTCWPM winds on L-II (11.6^{o}N and 114.4^{o}E) from 1800UTC on 20 November to 1800UTC on 21 November. TY Muifa was at this location at 1800UTC on 21 November. The arrow presents QTCWPM wind speed and direction.

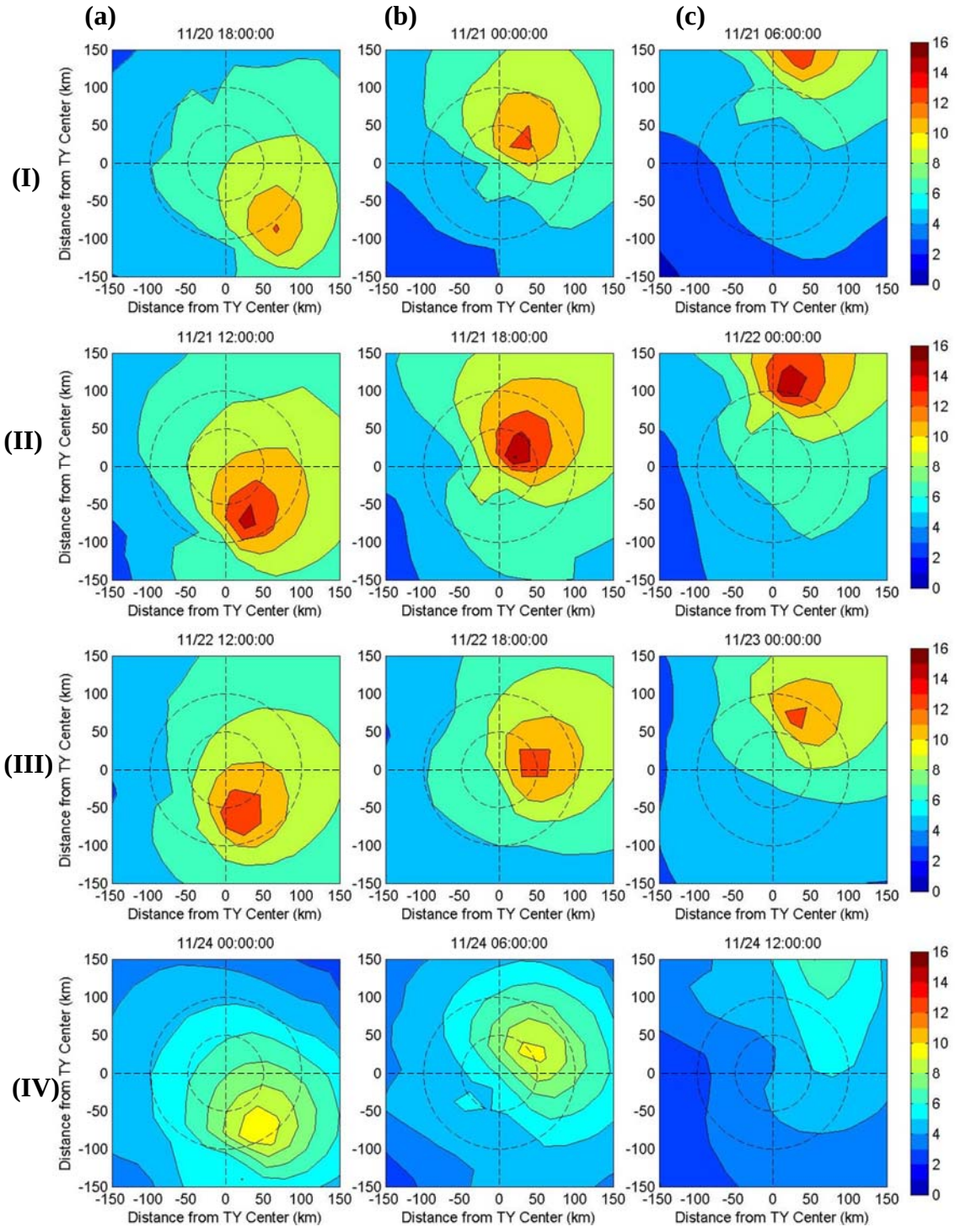

Fig. 15. Six-hourly evolutions of H_s at four locations (from vertical direction): (a) before typhoon arrivals (left column), (b) typhoon right on (central column), and (c) after typhoon departures (right column). The translation directions are rotated to northward.

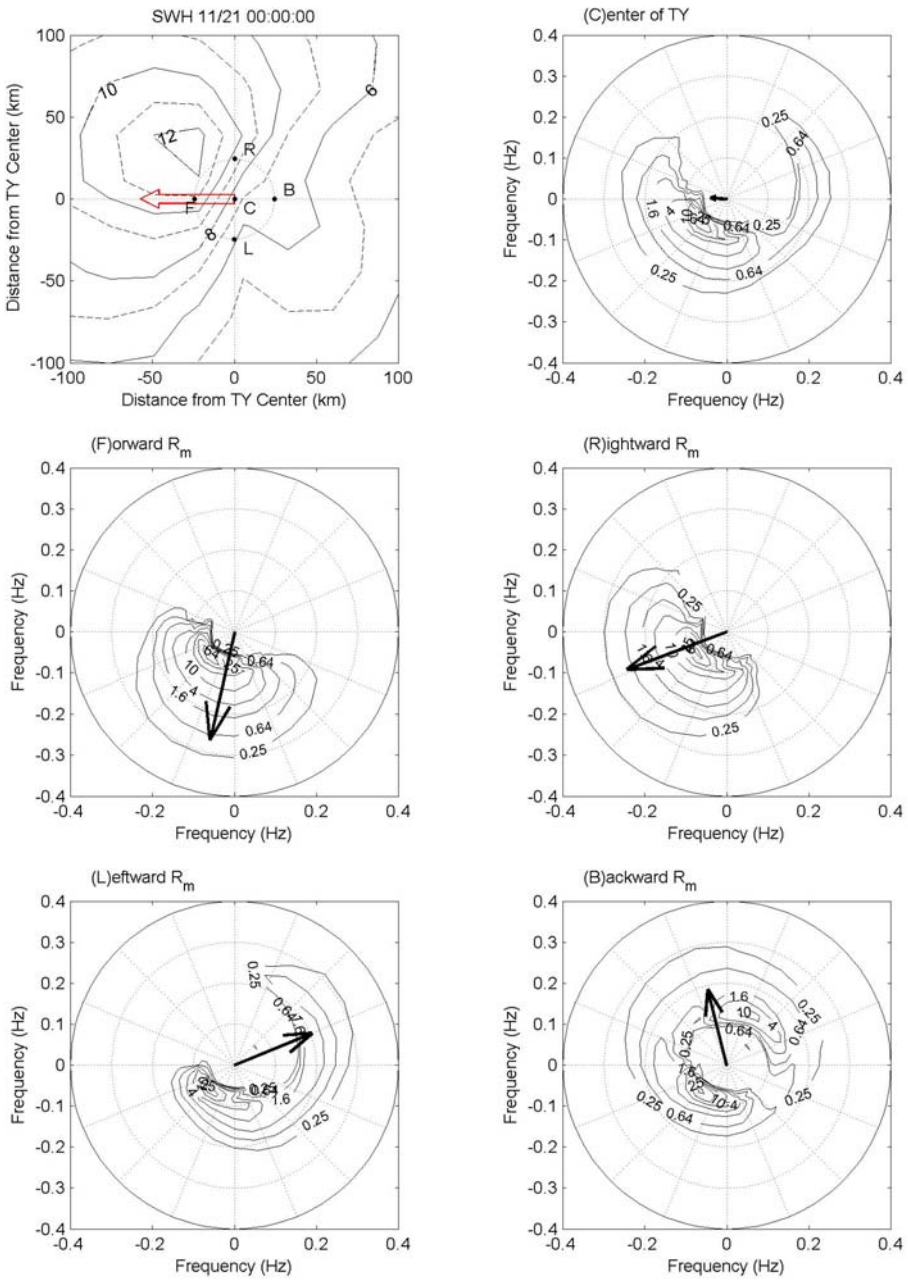

Figure 16. Wave characteristics at L-1 (11.9^{o}N, 117.2^{o}E, 0000UTC on 21 November): horizontal distribution of H_S and directional wave spectra at center (C) and four-way locations around the TY Muifa center with RMW away forward location (F), backward location (B), rightward location (R), and leftward location (L).

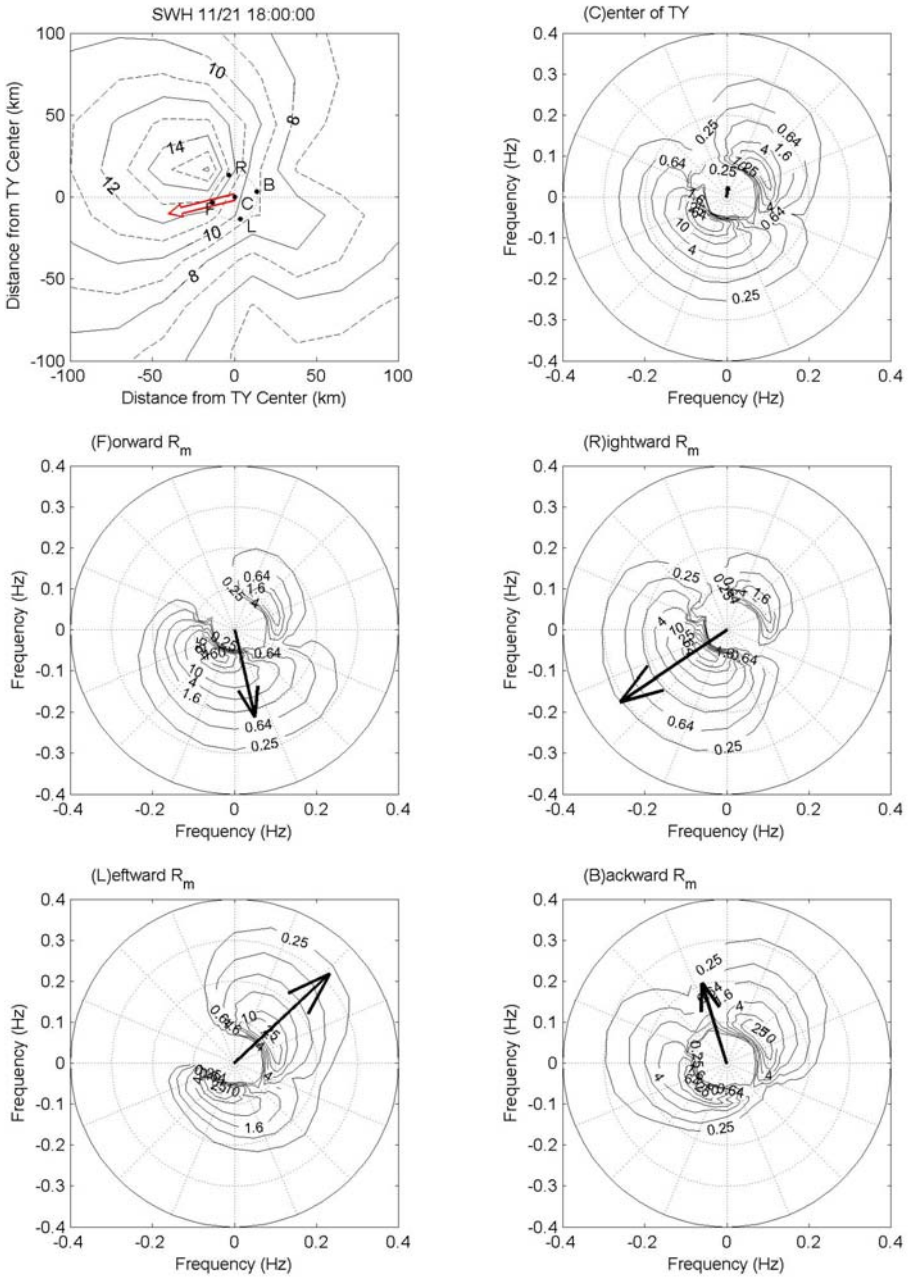

Figure 17. Wave characteristics at L-II (11.6°N, 114.4°E, 1800UTC on 21 November): horizontal distribution of H_S and directional wave spectra at center (C) and four-way locations around the TY Muifa center with RMW away forward location (F), backward location (B), rightward location (R), and leftward location (L).

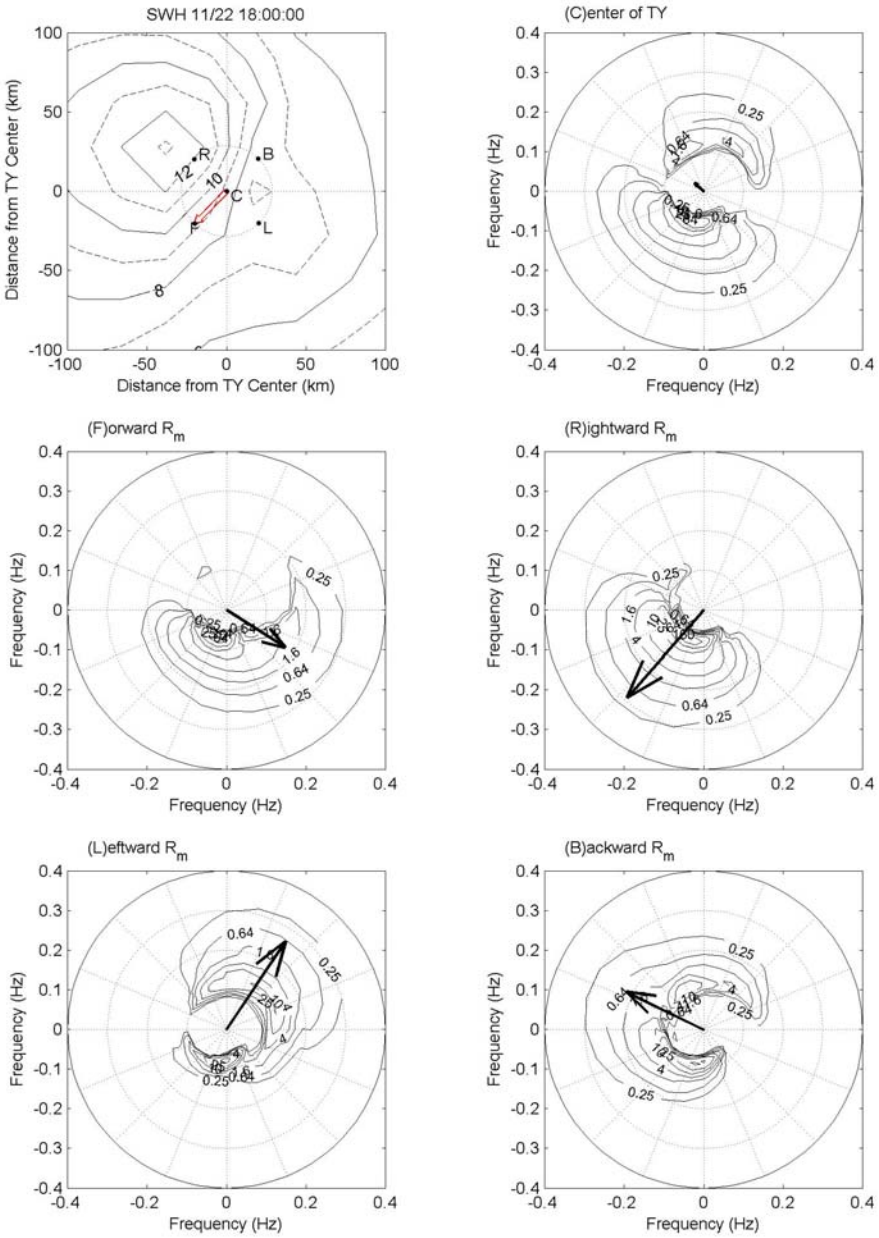

Figure 18. Wave characteristics at L-1II (10.5°N, 112.1°E, 1800UTC on 22 November): horizontal distribution of H_S and directional wave spectra at center (C) and four-way locations around the TY Muifa center with RMW away forward location (F), backward location (B), rightward location (R), and leftward location (L).

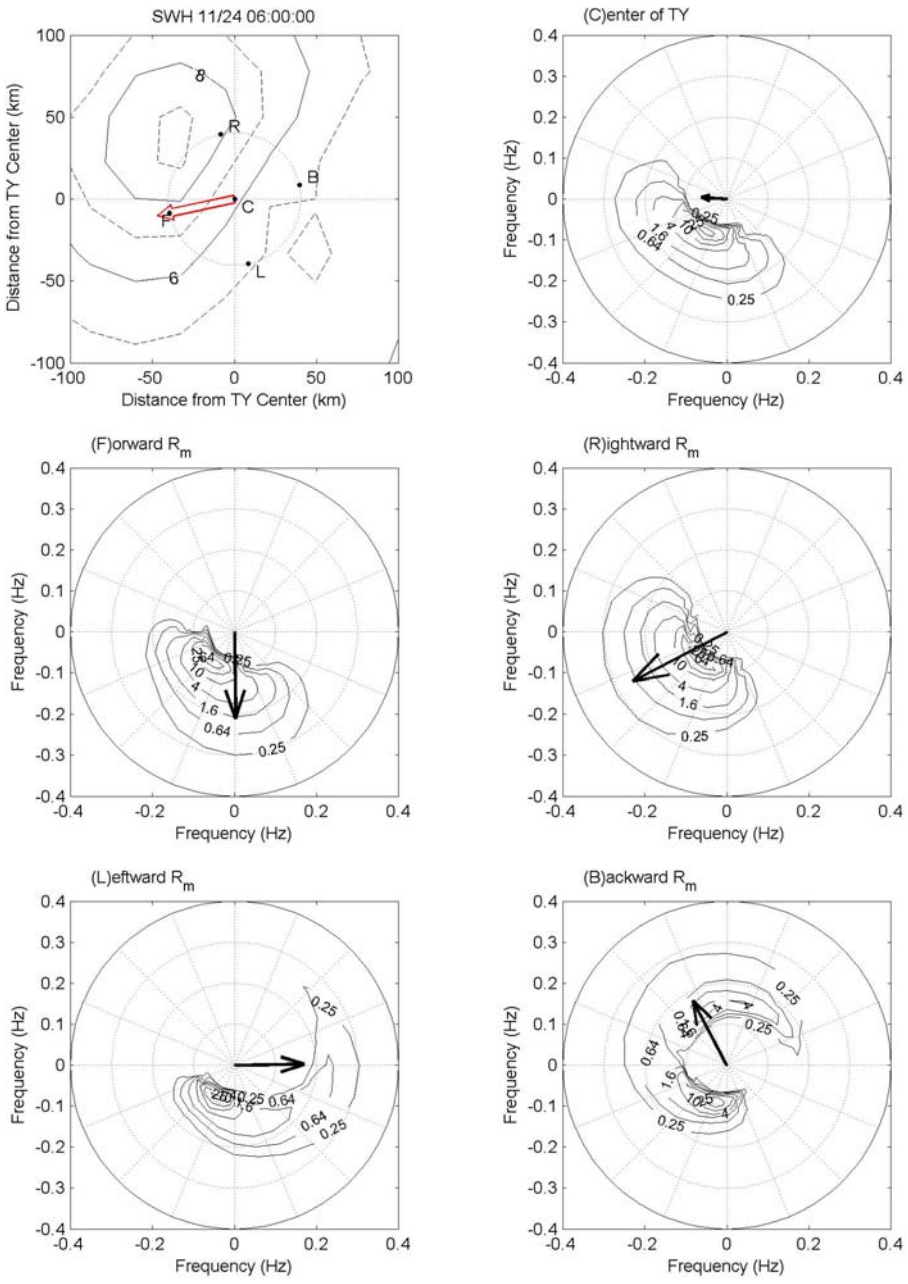

Figure 19. Wave characteristics at L-1II (8.8^{o}N, 108.8^{o}E, 0600UTC on 24 November): horizontal distribution of H_S and directional wave spectra at center (C) and four-way locations around the TY Muifa center with RMW away forward location (F), backward location (B), rightward location (R), and leftward location (L).